

Supplementary Material to “Adaptive Regularized Tri-Factor Non-Negative Matrix Factorization for Cell Type Deconvolution”

Tianyi Liu¹ Chuwen Liu¹ Quefeng Li^{1,*} Xiaojing Zheng^{1,2,*} Fei Zou^{1,3,*}

¹Department of Biostatistics, The University of North Carolina at Chapel Hill

²Department of Pediatrics, The University of North Carolina at Chapel Hill

³Department of Genetics, The University of North Carolina at Chapel Hill

A. Technical Assumptions

Before presenting the main results, we state the technical assumptions.

Assumption 1 (Initial conditions). (i) $\forall k, \exists j_k \in \{1, \dots, m\}$ such that $\theta_{j_k k}^0 > 0$; (ii) $\forall k, \exists i_k \in \{1, \dots, n\}$ such that $p_{k i_k}^0 > 0$. (iii) $\forall i' \in \{i_1, i_2, \dots, i_K\}, \forall j, Y_{j i'} > 0; \forall j' \in \{j_1, j_2, \dots, j_K\}, \forall i, Y_{j' i} > 0$.

Assumption 2 (Boundedness). (i) For any $1 \leq j \leq m$ and $1 \leq i \leq n$, $Y_{ji} \leq M_Y < \infty$. (ii) For any $1 \leq j \leq m$ and $1 \leq k \leq K_0$, $\Theta_{0 j_k} \leq M_\Theta < \infty$.

These assumptions are reasonable in practice. For every cell type with established reference expression, it is safe to assume that there exist some genes that display non-zero cell-type-specific expression, thereby fulfilling Assumption 1(i). For cell types lacking reference expression, an initial value in Θ^0 can be straightforwardly set to a positive value, thereby also satisfying the same assumption. Assumption 1(ii) is automatically satisfied due to how \mathbf{P}^0 is initialized in Algorithm 1. Assumption 1(iii) plays a pivotal role in ensuring that positive initialized values remain positive throughout the iterative process (see Supplementary Material Section B for details). This assumption is easy to verify and holds true unless the bulk expression matrix is excessively sparse, which is uncommon in practice. Assumption 2 is a mild assumption on upper bounds of gene expression.

B. The MU Steps

B.1. A Preliminary Lemma

Similar to [1], $f(\Theta, \mathbf{s}, \mathbf{P})$ is minimized using block-wise auxiliary functions that are quadratic over-estimators, which then leads to the MU steps in (4), (5), and (6). The claims

*Co-corresponding authors. Emails: quefeng@email.unc.edu (QL), xiaojinz@email.unc.edu (XZ), feizou@email.unc.edu (FZ).

that these updates will keep the positive initialized values positive will be investigated at the end of this section. An auxiliary function is defined next.

Definition 1 (Auxiliary function). *Given a vector space V and $\mathbf{v}, \mathbf{v}' \in V$, a function $g(\mathbf{v}|\mathbf{v}') : V \times V \mapsto \mathbb{R}$ is an auxiliary function for the function $f(\mathbf{v}) : V \mapsto \mathbb{R}$ at \mathbf{v}' if the following conditions are satisfied:*

$$g(\mathbf{v}|\mathbf{v}') \geq f(\mathbf{v}'), \forall \mathbf{v} \in V, \text{ and } g(\mathbf{v}'|\mathbf{v}') = f(\mathbf{v}').$$

As we shall see, the vector blocks in the auxiliary functions would be each row of Θ , each column of \mathbf{P} , and \mathbf{s} . To find the specific auxiliary functions for $f(\Theta, \mathbf{s}, \mathbf{P})$, a slightly modified form of a technical lemma given by [2] is needed and stated next. Its proof is also given in the same paper and thus omitted.

Lemma 1. *Given a positive semi-definite matrix $\mathbf{Q} \in \mathbb{R}_+^{b \times b}$ and $\mathbf{w} \in \mathbb{R}_+^b$, let $I \subseteq \{1, \dots, b\}$ be a set of indices such that $w_k > 0$ for any $k \in I$, $\mathbf{Q}_{II} \in \mathbb{R}_{++}^{|I| \times |I|}$, and $\mathbf{w}_I \in \mathbb{R}_{++}^{|I|}$ be the sub-matrix of \mathbf{Q} and the sub-vector of \mathbf{w} with indices in I , where $|I|$ denotes the cardinality of I . Then,*

$$\text{diag} \left\{ \frac{(\mathbf{Q}_{II}\mathbf{w}_I)}{\mathbf{w}_I} \right\} - \mathbf{Q}_{II} = \begin{bmatrix} \frac{(\mathbf{Q}_{II}\mathbf{w}_I)_1}{w_{I1}} & & \\ & \ddots & \\ & & \frac{(\mathbf{Q}_{II}\mathbf{w}_I)_{|I|}}{w_{I|I|}} \end{bmatrix} - \mathbf{Q}_{II}$$

is always positive semi-definite.

With Lemma 1, the auxiliary functions and multiplicative update (MU) steps are ready to be derived.

B.2. Derivations of The MU Steps

In addition to those in Section 2.1, we introduce two additional notation: for two square matrices of the same dimension, we write $\mathbf{A} \succ \mathbf{B}$ and $\mathbf{A} \succeq \mathbf{B}$ if $\mathbf{A} - \mathbf{B}$ is positive-definite and positive-semidefinite, respectively.

The auxiliary function and update step for each row $\boldsymbol{\theta}_j^\top$ is derived and then combined for $j = 1, \dots, m$ into the form of (4). For simplicity in notations, the index j is omitted in subscripts. The iteration number t is also omitted for \mathbf{s} and \mathbf{P} since both are treated as fixed. That is, we denote \mathbf{y}_j^\top as \mathbf{y}^\top , $\boldsymbol{\theta}_j^\top$ as $\boldsymbol{\theta}^\top$, and $\boldsymbol{\delta}_j^\top$ as $\boldsymbol{\delta}^\top$. We also define $\boldsymbol{\delta}_j^c = \mathbf{J} - \boldsymbol{\delta}_j$ for all j . Thus, for the j -th row of Θ , we can define the sub-problem of $f(\Theta, \mathbf{s}, \mathbf{P})$ as

$$\underset{\boldsymbol{\theta} \in \mathbb{R}_+^K}{\text{argmin}} \frac{1}{2mn} \|\mathbf{y}^\top - \boldsymbol{\theta}^\top \text{diag}(\mathbf{s}) \mathbf{P}\|_2^2 + \frac{\alpha_1}{2} \|\boldsymbol{\delta}^\top \odot (\boldsymbol{\theta}^\top - \boldsymbol{\theta}_0^\top)\|_2^2 + \frac{\alpha_2}{2} \|\boldsymbol{\delta}^{c\top} \odot \boldsymbol{\theta}^\top\|_2^2 + C_1(\mathbf{s}, \mathbf{P}) \quad (\text{S.1})$$

$$= \underset{\boldsymbol{\theta} \in \mathbb{R}_+^K}{\text{argmin}} \frac{1}{2mn} \|\mathbf{y}^\top - \mathbf{P}^\top \text{diag}(\mathbf{s}) \boldsymbol{\theta}\|_2^2 + \frac{\alpha_1}{2} \|\boldsymbol{\delta} \odot (\boldsymbol{\theta} - \boldsymbol{\theta}_0)\|_2^2 + \frac{\alpha_2}{2} \|\boldsymbol{\delta}^c \odot \boldsymbol{\theta}\|_2^2 + C_1(\mathbf{s}, \mathbf{P}), \quad (\text{S.2})$$

where $\text{diag}(\mathbf{s})$ and \mathbf{P} are treated as fixed and $C_1(\mathbf{s}, \mathbf{P})$ is a constant with respect to $\boldsymbol{\theta}$. We call the function in (S.2) $f_\theta(\boldsymbol{\theta})$. (S.2) is derived from (S.1) by transposing. Now, to

find the auxiliary function $h_\theta(\boldsymbol{\theta}|\boldsymbol{\theta}^t)$, by performing a second-order Taylor series expansion on $f_\theta(\boldsymbol{\theta})$ at $\boldsymbol{\theta} = \boldsymbol{\theta}^t$, we have

$$f_\theta(\boldsymbol{\theta}) = f_\theta(\boldsymbol{\theta}^t) + \nabla_{\boldsymbol{\theta}} f_\theta(\boldsymbol{\theta}^t)^\top (\boldsymbol{\theta} - \boldsymbol{\theta}^t) + \frac{1}{2} (\boldsymbol{\theta} - \boldsymbol{\theta}^t)^\top \nabla_{\boldsymbol{\theta}}^2 f_\theta(\boldsymbol{\theta}^t) (\boldsymbol{\theta} - \boldsymbol{\theta}^t).$$

Next, letting $\mathbf{V}(\boldsymbol{\delta}) = \text{diag}(\boldsymbol{\delta})$ and $\mathbf{V}^c(\boldsymbol{\delta}^c) = \text{diag}(\boldsymbol{\delta}^c)$, it can be observed that $\boldsymbol{\delta} \odot \boldsymbol{\theta} = \mathbf{V}\boldsymbol{\theta}$ and $\boldsymbol{\delta}^c \odot \boldsymbol{\theta} = \mathbf{V}^c\boldsymbol{\theta}$. Also, $\mathbf{V} + \mathbf{V}^c = \mathbf{I}$. The first and second derivatives of $f_\theta(\boldsymbol{\theta})$ are thus:

$$\nabla_{\boldsymbol{\theta}} f_\theta(\boldsymbol{\theta}) = \frac{1}{mn} \text{diag}(\mathbf{s}) \mathbf{P} (\mathbf{P}^\top \text{diag}(\mathbf{s}) \boldsymbol{\theta} - \mathbf{y}^\top) + \alpha_1 \mathbf{V}(\boldsymbol{\theta} - \boldsymbol{\theta}_0) + \alpha_2 \mathbf{V}^c \boldsymbol{\theta},$$

and

$$\nabla_{\boldsymbol{\theta}}^2 f_\theta(\boldsymbol{\theta}) = \frac{1}{mn} \text{diag}(\mathbf{s}) \mathbf{P} \mathbf{P}^\top \text{diag}(\mathbf{s}) + \alpha_1 \mathbf{V} + \alpha_2 \mathbf{V}^c.$$

It can be guaranteed $\nabla_{\boldsymbol{\theta}}^2 f_\theta(\boldsymbol{\theta}) \succ \mathbf{0}$ given $\alpha_1, \alpha_2 > 0$, as $\nabla_{\boldsymbol{\theta}}^2 f_\theta(\boldsymbol{\theta}) \succeq \alpha_1 \mathbf{V} + \alpha_2 \mathbf{V}^c \succeq \min(\alpha_1, \alpha_2) \mathbf{I} \succ \mathbf{0}$. Then, define $\mathbf{d}(\boldsymbol{\theta}^t) = \text{diag}(\boldsymbol{\theta}^t)^{-1} \nabla_{\boldsymbol{\theta}}^2 f_\theta(\boldsymbol{\theta}^t) \boldsymbol{\theta}^t$, and $\mathbf{D}(\boldsymbol{\theta}^t) = \text{diag}(\mathbf{d}(\boldsymbol{\theta}^t))$. Lemma 1 implies that, on coordinates that correspond to the positive elements of $\boldsymbol{\theta}$, $\mathbf{D}(\boldsymbol{\theta}^t) - \nabla_{\boldsymbol{\theta}}^2 f_\theta(\boldsymbol{\theta}^t) \succeq 0$. Define $\mathbb{R}_{++}^{K_1}$, where $K_1 \leq K$, as the open half space that contains this positive subset of $\boldsymbol{\theta}$. For simplification, we use the same notations for the full vectors and matrices on those positive coordinates. As mentioned in Section 2.2, we shall see that once a coordinate of $\boldsymbol{\theta}$ reaches zero, it stays zero thereafter, which justifies the focus on these positive coordinates. Next, define

$$h_\theta(\boldsymbol{\theta}|\boldsymbol{\theta}^t) = f_\theta(\boldsymbol{\theta}^t) + \nabla_{\boldsymbol{\theta}} f_\theta(\boldsymbol{\theta}^t)^\top (\boldsymbol{\theta} - \boldsymbol{\theta}^t) + \frac{1}{2} (\boldsymbol{\theta} - \boldsymbol{\theta}^t)^\top \mathbf{D}(\boldsymbol{\theta}^t) (\boldsymbol{\theta} - \boldsymbol{\theta}^t), \quad (\text{S.3})$$

which is an auxiliary function of (S.2) (thus of $f(\boldsymbol{\Theta}, \mathbf{s}, \mathbf{P})$ when we combine all subproblems together for $j = 1, \dots, m$). To demonstrate that it satisfies Definition 1, simply see that

$$h_\theta(\boldsymbol{\theta}|\boldsymbol{\theta}^t) - f_\theta(\boldsymbol{\theta}) = \frac{1}{2} (\boldsymbol{\theta} - \boldsymbol{\theta}^t)^\top (\mathbf{D}(\boldsymbol{\theta}^t) - \nabla_{\boldsymbol{\theta}}^2 f_\theta(\boldsymbol{\theta}^t)) (\boldsymbol{\theta} - \boldsymbol{\theta}^t) \geq 0, \quad \forall \boldsymbol{\theta}, \boldsymbol{\theta}^t \in \mathbb{R}_{++}^{K_1}$$

and due to Lemma 1 and that $h_\theta(\boldsymbol{\theta}^t|\boldsymbol{\theta}^t) - f_\theta(\boldsymbol{\theta}^t) = 0$, $\forall \boldsymbol{\theta}^t \in \mathbb{R}_{++}^{K_1}$. To derive the MU step from this auxiliary function, we find $\boldsymbol{\theta}^{t+1}$ such that

$$\boldsymbol{\theta}^{t+1} = \underset{\boldsymbol{\theta} \in \mathbb{R}_+^{K_1}}{\operatorname{argmin}} h_\theta(\boldsymbol{\theta}|\boldsymbol{\theta}^t). \quad (\text{S.4})$$

To guarantee the existence of a solution for (S.4), the feasible set of $\boldsymbol{\theta}$ is a closed space that includes 0. Since $\mathbf{D}(\boldsymbol{\theta}^t) - \nabla_{\boldsymbol{\theta}}^2 f_\theta(\boldsymbol{\theta}^t) \succeq 0$ and $\nabla_{\boldsymbol{\theta}}^2 f_\theta(\boldsymbol{\theta}^t) \succ 0$ by the assumptions, $\mathbf{D}(\boldsymbol{\theta}^t) \succ 0$, which implies that (S.3) is strictly convex. Thus, (S.3) has a global minimizer in the closed half space $\mathbb{R}_+^{K_1}$. By the optimality condition, if a feasible $\tilde{\boldsymbol{\theta}} \in \mathbb{R}_+^{K_1}$ satisfies $\nabla_{\boldsymbol{\theta}} h_\theta(\tilde{\boldsymbol{\theta}}|\boldsymbol{\theta}^t) = 0$, then $\tilde{\boldsymbol{\theta}}$ minimizes (S.3) globally and $\boldsymbol{\theta}^{t+1} = \tilde{\boldsymbol{\theta}}$ because of (S.4). Thus, we solve

$$\nabla_{\boldsymbol{\theta}} h_\theta(\boldsymbol{\theta}^{t+1}|\boldsymbol{\theta}^t) = \nabla_{\boldsymbol{\theta}} f_\theta(\boldsymbol{\theta}^t) + \mathbf{D}(\boldsymbol{\theta}^t)(\boldsymbol{\theta}^{t+1} - \boldsymbol{\theta}^t) = 0. \quad (\text{S.5})$$

Because $\mathbf{D}(\boldsymbol{\theta}^t)$ is diagonal, for each $k \in 1, \dots, K_1$, (S.5) implies

$$\theta_k^{t+1} = \theta_k^t - \frac{\nabla_{\boldsymbol{\theta}} f_\theta(\boldsymbol{\theta}^t)_k}{D(\boldsymbol{\theta}^t)_k}. \quad (\text{S.6})$$

We further simplify the notations by letting

$$\begin{aligned}
\nabla_{\boldsymbol{\theta}} f_{\boldsymbol{\theta}}(\boldsymbol{\theta}) &= \frac{1}{mn} \text{diag}(\mathbf{s}) \mathbf{P} (\mathbf{P}^\top \text{diag}(\mathbf{s}) \boldsymbol{\theta} - \mathbf{y}^\top) + \alpha_1 \mathbf{V} (\boldsymbol{\theta} - \boldsymbol{\theta}_0) + \alpha_2 \mathbf{V}^c \boldsymbol{\theta} \\
&= \left(\frac{1}{mn} \text{diag}(\mathbf{s}) \mathbf{P} \mathbf{P}^\top \text{diag}(\mathbf{s}) + \alpha_1 \mathbf{V} + \alpha_2 \mathbf{V}^c \right) \boldsymbol{\theta} \\
&\quad - \left(\frac{1}{mn} \text{diag}(\mathbf{s}) \mathbf{P} \mathbf{P}^\top \text{diag}(\mathbf{s}) \mathbf{y}^\top + \alpha_1 \mathbf{V} \boldsymbol{\theta}_0 \right) \\
&= \mathbf{A} \boldsymbol{\theta} - \mathbf{b}.
\end{aligned}$$

It follows immediately that $\nabla_{\boldsymbol{\theta}}^2 f_{\boldsymbol{\theta}}(\boldsymbol{\theta}) = \mathbf{A}$. Plugging in the values of $\nabla_{\boldsymbol{\theta}} f_{\boldsymbol{\theta}}(\boldsymbol{\theta}^t)_k$ and $D(\boldsymbol{\theta}^t)_k$ to (S.6), we have

$$\begin{aligned}
\theta_k^{t+1} &= \theta_k^t - \frac{(\mathbf{A} \boldsymbol{\theta}^t - \mathbf{b})_k}{\frac{1}{\theta_k^t} (\mathbf{A} \boldsymbol{\theta}^t)_k} \\
&= \theta_k^t - \frac{(\mathbf{A} \boldsymbol{\theta}^t)_k \theta_k^t}{(\mathbf{A} \boldsymbol{\theta}^t)_k} + \frac{b_k}{(\mathbf{A} \boldsymbol{\theta}^t)_k} \theta_k^t \\
&= \frac{b_k}{(\mathbf{A} \boldsymbol{\theta}^t)_k} \theta_k^t \\
&= \frac{\left(\frac{1}{mn} \text{diag}(\mathbf{s}) \mathbf{P} \mathbf{y}^\top + \alpha_1 \mathbf{V} \boldsymbol{\theta}_0 \right)_k}{\left[\left(\frac{1}{mn} \text{diag}(\mathbf{s}) \mathbf{P} \mathbf{P}^\top \text{diag}(\mathbf{s}) + \alpha_1 \mathbf{V} + \alpha_2 \mathbf{V}^c \right) \boldsymbol{\theta}^t \right]_k} \theta_k^t \\
&= \frac{\left(\text{diag}(\mathbf{s}) \mathbf{P} \mathbf{y}^\top + mn \alpha_1 \mathbf{V} \boldsymbol{\theta}_0 \right)_k}{\left[\left(\text{diag}(\mathbf{s}) \mathbf{P} \mathbf{P}^\top \text{diag}(\mathbf{s}) + mn (\alpha_1 \mathbf{V} + \alpha_2 \mathbf{V}^c) \right) \boldsymbol{\theta}^t \right]_k} \theta_k^t. \tag{S.7}
\end{aligned}$$

The multiplicative form of (S.7) guarantees that $\boldsymbol{\theta}^{t+1}$ is feasible. Therefore, $\boldsymbol{\theta}^{t+1}$ satisfies (S.4).

It is straightforward to check that (S.7) also applies to zero coordinates of $\boldsymbol{\theta}^t$ ($\{\theta_k^t : \theta_k^t \in \mathbb{R}_+^K \setminus \mathbb{R}_{++}^{K_1}\}$), as zero coordinates remain zero after any multiplication. Therefore, it is the unified update step for the entire $\boldsymbol{\theta}^t \in \mathbb{R}_+^K$. Since it corresponds to the update for the (j, k) -th element in $\boldsymbol{\Theta}$, combining all elements gives (4).

We remark that (S.6) reflects the block coordinate descent nature of the multiplicative update in $\boldsymbol{\Theta}$, as observed by [4]. In fact, the update steps for \mathbf{P} and $\text{diag}(\mathbf{s})$ can be written in similar fashions.

The update step for \mathbf{P} in (5) can be similarly derived as that for $\boldsymbol{\Theta}$. We begin with specifying the sub-problem for \mathbf{p}_i , $i = 1, \dots, n$, treating $\boldsymbol{\Theta}$ and $\text{diag}(\mathbf{s})$ as fixed and omitting the subscripts and the iteration number (t for \mathbf{s} and $t+1$ for $\boldsymbol{\Theta}$) for convenience in notations:

$$\underset{\mathbf{p} \in \mathbb{R}_+^K}{\operatorname{argmin}} f_p(\mathbf{p}) = \frac{1}{2mn} \|\mathbf{y} - \boldsymbol{\Theta} \text{diag}(\mathbf{s}) \mathbf{p}\|_2^2 + \frac{\beta}{2} \boldsymbol{\rho}^{-1} \|\mathbf{p} - \mathbf{m}\|_2^2 + K_2(\boldsymbol{\Theta}, \mathbf{s}), \tag{S.8}$$

where $K_2(\boldsymbol{\Theta}, \mathbf{s})$ only depends on $\boldsymbol{\Theta}$ and \mathbf{s} and is a constant with respect to \mathbf{P} . Then, its first and second derivatives with respect to \mathbf{p} are

$$\begin{aligned}
\nabla_{\mathbf{p}} f_p(\mathbf{p}) &= \left(\frac{1}{mn} \text{diag}(\mathbf{s}) \boldsymbol{\Theta}^\top \boldsymbol{\Theta} \text{diag}(\mathbf{s}) + \beta \boldsymbol{\rho}^{-1} \right) \mathbf{p} - \left(\frac{1}{mn} \text{diag}(\mathbf{s}) \boldsymbol{\Theta}^\top \mathbf{y} + \beta \boldsymbol{\rho}^{-1} \mathbf{m} \right) \\
&= \mathbf{C} \mathbf{p} - \mathbf{q},
\end{aligned} \tag{S.9}$$

and

$$\nabla_{\mathbf{p}}^2 f_p(\mathbf{p}) = \frac{1}{mn} \text{diag}(\mathbf{s}) \boldsymbol{\Theta}^\top \boldsymbol{\Theta} \text{diag}(\mathbf{s}) + \beta \boldsymbol{\rho}^{-1} = \mathbf{C}. \quad (\text{S.10})$$

To find the auxiliary function of (S.8), define $\mathbf{d}(\mathbf{p}^t) = \text{diag}(\mathbf{p}^t)^{-1} \nabla_{\mathbf{p}}^2 f_p(\mathbf{p}^t) \mathbf{p}^t$, and $\mathbf{D}(\mathbf{p}^t) = \text{diag}(\mathbf{d}(\mathbf{p}^t))$, and

$$h_p(\mathbf{p}|\mathbf{p}^t) = f_p(\mathbf{p}^t) + \nabla_{\mathbf{p}} f_p(\mathbf{p}^t)^\top (\mathbf{p} - \mathbf{p}^t) + \frac{1}{2} (\mathbf{p} - \mathbf{p}^t)^\top \mathbf{D}(\mathbf{p}^t) (\mathbf{p} - \mathbf{p}^t). \quad (\text{S.11})$$

On the $K_2 \leq K$ positive coordinates in \mathbf{p}^t , (S.11) is the auxiliary function of (S.8) due to Lemma 1. The verification is the same to that for $h_\theta(\boldsymbol{\theta}|\boldsymbol{\theta}^t)$ and omitted here. Next, we find \mathbf{p}^{t+1} such that

$$\mathbf{p}^{t+1} = \underset{\mathbf{p} \in \mathbb{R}_+^{K_2}}{\operatorname{argmin}} h_p(\mathbf{p}|\mathbf{p}^t).$$

This in turn corresponds to finding \mathbf{p}^{t+1} such that

$$\nabla_{\mathbf{p}} h_p(\mathbf{p}^{t+1}|\mathbf{p}^t) = \nabla_{\mathbf{p}} f_p(\mathbf{p}^t) + \mathbf{D}(\mathbf{p}^t)(\mathbf{p}^{t+1} - \mathbf{p}^t) = 0,$$

given that such a \mathbf{p}^{t+1} is feasible. After some algebra, for any $k = 1, \dots, K_2$,

$$\begin{aligned} p_k^{t+1} &= \frac{q_k}{(\mathbf{C}\mathbf{p}^t)_k} p_k^t \\ &= \frac{\left(\frac{1}{mn} \text{diag}(\mathbf{s}) \boldsymbol{\Theta}^\top \mathbf{y} + \beta \boldsymbol{\rho}^{-1} \mathbf{m} \right)_k}{\left\{ \left(\frac{1}{mn} \text{diag}(\mathbf{s}) \boldsymbol{\Theta}^\top \boldsymbol{\Theta} \text{diag}(\mathbf{s}) + \beta \boldsymbol{\rho}^{-1} \right) \mathbf{p} \right\}_k} p_k^t \\ &= \frac{\left(\text{diag}(\mathbf{s}) \boldsymbol{\Theta}^\top \mathbf{y} + mn\beta \boldsymbol{\rho}^{-1} \mathbf{m} \right)_k}{\left\{ \left(\text{diag}(\mathbf{s}) \boldsymbol{\Theta}^\top \boldsymbol{\Theta} \text{diag}(\mathbf{s}) + mn\beta \boldsymbol{\rho}^{-1} \right) \mathbf{p} \right\}_k} p_k^t, \end{aligned} \quad (\text{S.12})$$

which produces a feasible \mathbf{p}^{t+1} . Moreover, (S.12) also applies to the zero coordinates in \mathbf{p}^t . Since (S.12) corresponds to the update step for the (k, i) -th element for the \mathbf{P} matrix, combining all of these elements yields (5).

Deriving the updates step for $\text{diag}(\mathbf{s})$ in (6) largely follows the same footsteps as for $\boldsymbol{\Theta}$ and \mathbf{P} . To find a suitable sub-problem, we start from the following identity

$$\boldsymbol{\Theta} \text{diag}(\mathbf{s}) \mathbf{P} = \boldsymbol{\Theta} \text{diag}(\mathbf{s}) \mathbf{P} = \sum_{k=1}^K s_k \boldsymbol{\theta}_k \mathbf{p}_k^\top. \quad (\text{S.13})$$

Denoting $\mathbf{G}_k = \boldsymbol{\theta}_k \mathbf{p}_k^\top$ and only assuming \mathbf{s} a variable, we transform the objective function

in $f(\Theta, \mathbf{s}, \mathbf{P})$ with respect to \mathbf{s} as follows

$$\begin{aligned}
f_s(\mathbf{s}) &= \frac{1}{2mn} \|\mathbf{Y} - \Theta \text{diag}(\mathbf{s}) \mathbf{P}\|_F^2 + C_3(\Theta, \mathbf{P}) && \text{(by rewriting } f(\Theta, \mathbf{s}, \mathbf{P})) \\
&= \frac{1}{2mn} \|\mathbf{Y} - \sum_{k=1}^K s_k \mathbf{G}_k\|_F^2 + C_3(\Theta, \mathbf{P}) && \text{(by (S.13))} \\
&\propto \frac{1}{2} \left\{ \sum_{k=1}^K s_k^2 \text{tr}(\mathbf{G}_k^\top \mathbf{G}_k) - 2 \sum_{k=1}^K s_k \text{tr}(\mathbf{G}_k^\top \mathbf{Y}) + \sum_{k \neq l} s_k s_l \text{tr}(\mathbf{G}_k^\top \mathbf{G}_l) \right\} + C'_3(\Theta, \mathbf{P}) \\
&\quad \text{(by expanding the squared Frobenius norm and dropping } m, n) \\
&= \frac{1}{2} \left\{ \sum_{k=1}^K s_k^2 \text{tr}(\mathbf{G}_k^\top \mathbf{G}_k) + \sum_{k \neq l} s_k s_l \text{tr}(\mathbf{G}_k^\top \mathbf{G}_l) \right\} - \sum_{k=1}^K s_k \text{tr}(\mathbf{G}_k^\top \mathbf{Y}) + C'_3(\Theta, \mathbf{P}) \\
&\quad \text{(by rearranging the last step)} \\
&= \frac{1}{2} \mathbf{s}^\top \mathbf{Z} \mathbf{s} - \mathbf{u}^\top \mathbf{s} + C'_3(\Theta, \mathbf{P}),
\end{aligned} \tag{S.14}$$

where $\mathbf{Z} \in \mathbb{R}_{++}^{K \times K}$, $Z_{ij} = \text{tr}(\mathbf{G}_i^\top \mathbf{G}_j) = \text{tr}(\mathbf{p}_i \boldsymbol{\theta}_i^\top \boldsymbol{\theta}_j \mathbf{p}_j^\top)$, $\mathbf{u} \in \mathbb{R}_{++}^K$, and $u_k = \text{tr}(\mathbf{Y}^\top \mathbf{G}_k) = \text{tr}(\mathbf{Y}^\top \boldsymbol{\theta}_k \mathbf{p}_k^\top)$. Both C_3 and C'_3 only depend on Θ and \mathbf{P} , hence are constant with respect to \mathbf{s} . (S.14) is then our sub-problem for \mathbf{s} . From (S.14), the first and second derivatives for \mathbf{s} are $\nabla_{\mathbf{s}} f_s(\mathbf{s}) = \mathbf{Z} \mathbf{s} - \mathbf{u}$, and $\nabla_{\mathbf{s}}^2 f_s(\mathbf{s}) = \mathbf{Z}$. Again, define $\mathbf{d}(\mathbf{s}^t) = \text{diag}(\mathbf{s}^t)^{-1} \nabla_{\mathbf{s}}^2 f_s(\mathbf{s}^t) \mathbf{s}^t$, $\mathbf{D}(\mathbf{s}^t) = \text{diag}(\mathbf{d}(\mathbf{s}^t))$, and

$$h_s(\mathbf{s} | \mathbf{s}^t) = f_s(\mathbf{s}^t) + \nabla_{\mathbf{s}} f_s(\mathbf{s}^t)^\top (\mathbf{s} - \mathbf{s}^t) + \frac{1}{2} (\mathbf{s} - \mathbf{s}^t)^\top \mathbf{D}(\mathbf{s}^t) (\mathbf{s} - \mathbf{s}^t). \tag{S.15}$$

(S.15) is an auxiliary function of $f(\Theta, \mathbf{s}, \mathbf{P})$ for \mathbf{s} according to Lemma 1. Since $\mathbf{s} \in \mathbb{R}_{++}^K$, there is no need for sub-setting to positive coordinates. Thus, we obtain \mathbf{s}^{t+1} by finding a feasible

$$\mathbf{s}^{t+1} = \underset{\mathbf{s} \in \mathbb{R}_{++}^K}{\operatorname{argmin}} h_s(\mathbf{s} | \mathbf{s}^t). \tag{S.16}$$

We remark that this is a slight relaxation of the problem to update \mathbf{s} , since it is originally assumed that $\mathbf{s} \in \mathbb{R}_{++}^K$. However, this allows us to obtain a guaranteed closed form global minimizer for (S.16) in the closed half space \mathbb{R}_{++}^K , and the resulting update satisfies is feasible in \mathbb{R}_{++}^K as long as not all values of $\boldsymbol{\theta}_k$ or \mathbf{p}_k^\top are 0 for any $k = 1, \dots, K$, which is stated as Assumption 1(i) and 1(ii). (S.16) leads to solving

$$\nabla_{\mathbf{s}} h_s(\mathbf{s}^{t+1} | \mathbf{s}^t) = \nabla_{\mathbf{s}} f_s(\mathbf{s}^t) + \mathbf{D}(\mathbf{s}^t) (\mathbf{s}^{t+1} - \mathbf{s}^t) = 0,$$

from which we have

$$s_k^{t+1} = \frac{u_k}{(\mathbf{Z} \mathbf{s}^t)_k} s_k^t. \tag{S.17}$$

(S.17) corresponds to the update for the k -th coordinate in (6), which yields feasible s_k^{t+1} under the assumptions, since $Z_{ij} = \text{tr}(\mathbf{G}_i^\top \mathbf{G}_j) = (\boldsymbol{\theta}_i^\top \boldsymbol{\theta}_j) \text{tr}(\mathbf{p}_i \mathbf{p}_j^\top)$, and $u_k = \text{tr}(\mathbf{Y}^\top \mathbf{G}_k) = \text{tr}(\mathbf{Y}^\top \boldsymbol{\theta}_k \mathbf{p}_k^\top)$. Moreover,

$$Z_{ij} = \text{tr}(\mathbf{p}_i \boldsymbol{\theta}_i^\top \boldsymbol{\theta}_j \mathbf{p}_j^\top) = (\boldsymbol{\theta}_i^\top \boldsymbol{\theta}_j) (\mathbf{p}_j^\top \mathbf{p}_i), \tag{S.18}$$

and that

$$u_k = \text{tr}(\mathbf{Y}^\top \boldsymbol{\theta}_k \mathbf{p}_k^\top) = \sum_{j=1}^m \sum_{i=1}^n y_{ji} \theta_{jk} p_{ki}. \tag{S.19}$$

For the denominator in (S.17), we see that

$$(\mathbf{Z}\mathbf{s}^t)_k = \sum_{l=1}^K Z_{kl} s_l^t \geq Z_{kk} s_k^t = \|\boldsymbol{\theta}_k\|_2^2 \|\mathbf{p}_k\|_2^2 s_k^t > 0, \quad (\text{S.20})$$

where the last step is a result of (S.18) and the stability of updates based Assumption 1(i) and 1(ii), which will be discussed in details below. As for the numerator of (S.17), taking from the stability of updates due to Assumption 1(i) and 1(ii) and assuming $\theta_{j_k k} > 0$ and $p_{ki_k} > 0$, by (S.19), we have

$$u_k = \sum_{j=1}^m \sum_{i=1}^n y_{ji} \theta_{jk} p_{ki} \geq y_{j_k i_k} \theta_{j_k k} p_{ki_k} > 0,$$

as long as $y_{j_k i_k} > 0$. Given Assumption 1(iii), we conclude that $\mathbf{s}^{t+1} \in \mathbb{R}_{++}^K$.

B.3. Stability of The Update Steps

To justify the claim that for any j and k , $\theta_{jk}^{t+1} > 0$ whenever $\theta_{jk}^t > 0$ for $t = 0, 1, 2, \dots$, notice that the denominator of (S.7) is automatically positive whenever $\alpha_1, \alpha_2 > 0$. For guaranteeing that its numerator is also positive, we want to show

$$(\text{diag}(\mathbf{s}^t) \mathbf{P}^t \mathbf{y}_j^\top)_k = s_k^t \sum_{i=1}^n p_{ki}^t y_{ji} \geq s_k^t p_{ki_k}^t y_{j_k i_k} > 0, \quad (\text{S.21})$$

where the index i_k is defined as in Assumption 1(ii). By Assumption 1(iii), $y_{j_k i_k} > 0$, and $s_k^t > 0$ as discussed above. Thus, (S.21) holds whenever $p_{ki_k}^t > 0$. Similarly, for proving the claim that for any k and i , $p_{ki}^{t+1} > 0$ whenever $p_{ki}^t > 0$, notice that the denominator for (S.12) is also positive whenever $\beta > 0$. To prove that its numerator is positive, we need to show

$$(\text{diag}(\mathbf{s}^t) (\boldsymbol{\Theta}^{t+1})^\top \mathbf{y}_i)_k = s_k^t \sum_{j=1}^m \theta_{jk}^{t+1} y_{ji} \geq s_k^t \theta_{j_k k}^{t+1} y_{j_k i_k} > 0, \quad (\text{S.22})$$

where j_k is defined as in Assumption 1(i). (S.22) holds whenever $\theta_{j_k k}^{t+1} > 0$.

Since by Assumption 1(ii) and Assumption 1(i), $p_{ki_k}^0 > 0$ and $\theta_{j_k k}^0 > 0$. Therefore, we can show that $p_{ki_k}^t > 0$ and $\theta_{j_k k}^{t+1} > 0$ for any $t = 0, 1, 2, \dots$ by induction through (S.21) and (S.22). Thus, the claims on the stability of updates hold.

C. Proof of Theorem 1

To prove Theorem 1, we leverage on the convergence properties of the block successive upper-bound minimization (BSUM) algorithms proved by [3]. Namely, we can view Algorithm 1 as a BSUM algorithm by counting a total of $m + n + 1$ separate blocks which the algorithm minimizes successively: m for updating $\boldsymbol{\Theta}^t$, n for \mathbf{P}^t , and one for \mathbf{s}^t . To utilize such properties, we need to prove the following proposition, which states the conditions on the update steps' auxiliary functions for Algorithm 1 to formally qualify as BSUM, which is translated from Assumption 2 of [3]:

Proposition 1 (Algorithm 1 is BSUM). $h_\theta(\boldsymbol{\theta}_j|\boldsymbol{\theta}_j^t)$, $h_p(\mathbf{p}_i|\mathbf{p}_i^t)$, and $h_s(\mathbf{s}|\mathbf{s}^t)$ satisfy the following conditions for any $j = 1, 2, \dots, m$ and $i = 1, 2, \dots, n$: (1) $h_{\theta_j}(\boldsymbol{\theta}_j|\boldsymbol{\theta}_j^t) \geq f_\theta(\boldsymbol{\theta}_j^t)$; $h_p(\mathbf{p}_i|\mathbf{p}_i^t) \geq f_p(\mathbf{p}_i^t)$; $h_s(\mathbf{s}|\mathbf{s}^t) \geq f_s(\mathbf{s}^t)$; (2) $h_{\theta_j}(\boldsymbol{\theta}_j|\boldsymbol{\theta}_j^t)$, $h_p(\mathbf{p}_i|\mathbf{p}_i^t)$, and $h_s(\mathbf{s}|\mathbf{s}^t)$ are continuous on their domains; (3) Any directional derivative of $h_{\theta_j}(\boldsymbol{\theta}_j|\boldsymbol{\theta}_j^t)$, $h_p(\mathbf{p}_i|\mathbf{p}_i^t)$, and $h_s(\mathbf{s}|\mathbf{s}^t)$ within their domains are equal to the direactional derivative of $f_\theta(\boldsymbol{\theta}_j^t)$, $f_p(\mathbf{p}_i^t)$, and $f_s(\mathbf{s}^t)$ respectively.

Proof. The proof is quite straightforward. (1) and (2) are direct from the construction of the surrogate functions and Lemma 1, which also manifests the majorization-minimization (MM) property [5] of each block's update. (3) is seen by differentiating (S.3), (S.11), and (S.15), which leads to $\nabla_{\boldsymbol{\theta}_j} h_\theta(\boldsymbol{\theta}_j^t|\boldsymbol{\theta}_j^t) = \nabla_{\boldsymbol{\theta}_j} f_\theta(\boldsymbol{\theta}_j^t)$, $\forall j$, $\nabla_{\mathbf{p}_i} h_p(\mathbf{p}_i^t|\mathbf{p}_i^t) = \nabla_{\mathbf{p}_i} f_p(\mathbf{p}_i^t)$, $\forall i$, and $\nabla_{\mathbf{s}} h_s(\mathbf{s}^t|\mathbf{s}^t) = \nabla_{\mathbf{s}} f_s(\mathbf{s}^t)$. Equal gradients automatically guarantee equal directional derivatives, proving the proposition. \square

Now that Algorithm 1 is found to be BSUM, Theorem 1 can be proved directly by the results of Theorem 2(b) in [3]. But a few additional conditions presented in the following propositions need to be verified, both of which are proved thereafter.

Proposition 2 (Compact Sub-level Sets). *The sub-level set $\mathcal{X}^0 : \{(\boldsymbol{\Theta}, \mathbf{s}, \mathbf{P}) : f(\boldsymbol{\Theta}, \mathbf{s}, \mathbf{P}) \leq f(\boldsymbol{\Theta}^0, \mathbf{s}^0, \mathbf{P}^0)\}$ of $f(\boldsymbol{\Theta}, \mathbf{s}, \mathbf{P})$ given the update steps in Algorithm 1 is compact.*

Proposition 3 (Unique Global Minimizer of Auxiliary Functions). *Given Assumption 1, $\forall t \in \mathbb{R}_+$ and for all i and j , the auxiliary functions $h_\theta(\boldsymbol{\theta}_j|\boldsymbol{\theta}_j^t)$, $h_p(\mathbf{p}_i|\mathbf{p}_i^t)$, and $h_s(\mathbf{s}|\mathbf{s}^t)$ each have a unique global minimizer in \mathbb{R}_+^K .*

C.1. Proof of Proposition 2

We first introduce the definition of coercive functions through:

Definition 2 (Coercivity). *A function $f(\mathbf{X}_1, \dots, \mathbf{X}_N) : V_1 \times \dots \times V_N \rightarrow \mathbb{R}$, where V_i is a Euclidean vector space endorsed with the L_2 norm if its elements are vectors or with the Frobenius norm if the elements are matrices, is called coercive if $\forall i$, $\|\mathbf{X}_i\| \rightarrow \infty$ implies $f(\mathbf{X}_1, \dots, \mathbf{X}_N) \rightarrow \infty$.*

In fact, continuous coercive functions always have compact sub-level sets, as shown by the following lemma:

Lemma 2. *If a continuous function $f(\mathbf{X}_1, \dots, \mathbf{X}_N) : V_1 \times \dots \times V_N \rightarrow \mathbb{R}$ is jointly coercive, then its sublevel set $\mathcal{X}^r := \{(\mathbf{X}_1, \dots, \mathbf{X}_N) : f(\mathbf{X}_1, \dots, \mathbf{X}_N) \leq r\}$ is compact for any $r \in \mathbb{R}$.*

Proof. Because f is continuous and the space $f(\mathbf{X}_1, \dots, \mathbf{X}_n) \leq r$ is closed, \mathcal{X}^r is closed. We prove the boundedness of \mathcal{X}^r by contrapositive. We let $\mathcal{X}^r = \mathcal{X}_1^r \times \dots \times \mathcal{X}_N^r$, where $\mathcal{X}_i^r \subseteq V_i$. If \mathcal{X}^r is unbounded, then one of \mathcal{X}_i^r is unbounded. If \mathcal{X}_i^r is unbounded, we can find a sequence of $\{\mathbf{X}_k\}_{k=1}^\infty$ such that $\|\mathbf{X}_k\| \rightarrow \infty$ as $k \rightarrow \infty$, which implies f is not jointly coercive. Therefore, whenever f is jointly coercive, $\mathcal{X}^r = \mathcal{X}_1^r \times \dots \times \mathcal{X}_N^r$ is bounded. Since Euclidean spaces admit the Heine-Borel property, \mathcal{X}^r is compact. \square

Coming back to the proof of Proposition 2, it is easy to check that $f(\boldsymbol{\Theta}, \mathbf{s}, \mathbf{P})$ is continuously differentiable. To prove that it is also coercive, we need to show that $f(\boldsymbol{\Theta}, \mathbf{s}, \mathbf{P})$ tends to ∞ whenever $\|\boldsymbol{\Theta}\|_F$, $\|\mathbf{s}\|_2$, or $\|\mathbf{P}\|_F$ does so.

Beginning with the case for Θ , we have, by $f(\Theta, s, P)$,

$$\begin{aligned}
f(\Theta, s, P) &\geq \frac{\alpha_1}{2} \|\Delta \odot \Theta - \Theta_0\|_F^2 + \frac{\alpha_2}{2} \|\Delta^c \odot \Theta\|_F^2 \\
&\geq \min\left(\frac{\alpha_1}{2}, \frac{\alpha_2}{2}\right) (\|\Delta \odot \Theta - \Theta_0\|_F^2 + \|\Delta^c \odot \Theta\|_F^2) \\
&\geq \min\left(\frac{\alpha_1}{2}, \frac{\alpha_2}{2}\right) (\|\Delta \odot \Theta\|_F^2 - \|\Theta_0\|_F^2 + \|\Delta^c \odot \Theta\|_F^2) \\
&= \min\left(\frac{\alpha_1}{2}, \frac{\alpha_2}{2}\right) (\|\Theta\|_F^2 - \|\Theta_0\|_F^2) \\
&= \min\left(\frac{\alpha_1}{2}, \frac{\alpha_2}{2}\right) \|\Theta\|_F^2 \left(1 - \frac{\|\Theta_0\|_F^2}{\|\Theta\|_F^2}\right). \tag{S.23}
\end{aligned}$$

Since $\min\left(\frac{\alpha_1}{2}, \frac{\alpha_2}{2}\right) > 0$ and $\frac{\|\Theta_0\|_F^2}{\|\Theta\|_F^2} \leq \frac{mK_0M_\Theta}{\|\Theta\|_F^2} \rightarrow 0$ as $\|\Theta\|_F \rightarrow \infty$ by Assumption 2, (S.23) then guarantees that $f(\Theta, s, P) \rightarrow \infty$ when $\|\Theta\|_F \rightarrow \infty$.

In the case for P , whenever $\|P\|_F \rightarrow \infty$, there is a k such that \mathbf{p}_k^\top satisfies $\|\mathbf{p}_k^\top\|_2 \rightarrow \infty$. Also, since $\mathbf{p}_k \in \mathbb{R}_+^n$, there exists a column indexed i_k as defined in Assumption 1(ii) such that $p_{ki_k} \rightarrow \infty$. Then,

$$\begin{aligned}
f(\Theta, s, P) &\geq \frac{\beta}{2} \sum_{l=1}^K r_l^{-1} \|\mathbf{p}_l^\top - \mathbf{m}_l\|_2^2 \geq \frac{\beta}{2} r_k^{-1} \|\mathbf{p}_k^\top - \mathbf{m}_k\|_2^2 \\
&= \frac{\beta}{2} r_k^{-1} \sum_{i=1}^n (p_{ki} - \nu_k)^2 \geq \frac{\beta}{2} r_k^{-1} (p_{ki_k} - \nu_k)^2 \rightarrow \infty,
\end{aligned}$$

as ν_k is assumed fixed and $\beta > 0$.

Lastly for s , we can similarly argue that, because $s \in \mathbb{R}_{++}^K$, $\|s\|_2 \rightarrow \infty$ implies there is a k such that $s_k \rightarrow \infty$. From the steps leading to (S.14), we have

$$\begin{aligned}
f(\Theta, s, P) &\geq \frac{1}{2mn} \|\mathbf{Y} - \Theta \text{diag}(s) \mathbf{P}\|_F^2 = \frac{1}{2mn} \|\mathbf{Y} - \sum_{k=1}^K s_k \mathbf{G}_k\|_F^2 \\
&\geq \frac{1}{2mn} \left(\left\| \sum_{l=1}^K s_l \mathbf{G}_l \right\|_F^2 - \|\mathbf{Y}\|_F^2 \right) \\
&= \frac{1}{2mn} (s_k \|\mathbf{G}_k\|_F^2 - \|\mathbf{Y}\|_F^2) \rightarrow \infty.
\end{aligned}$$

The last line is because $\|\mathbf{G}_k\| > 0$ due to Assumption 1(i) and Assumption 1(ii) and that $\|\mathbf{Y}\|_F \leq mnM_Y < \infty$ by Assumption 2. Combining the cases for Θ , P , and s completes the proof that $f(\Theta, s, P)$ is coercive.

Since $f(\Theta, s, P)$ is continuous and coercive, the set $\mathcal{X}^0 : \{(\Theta, s, P) : f(\Theta, s, P) \leq f(\Theta^0, s^0, P^0)\}$ is compact according to Lemma 2. We have concluded the proof of Proposition 2.

C.2. Proof of Proposition 3

Since $h_\theta(\theta_j | \theta_j^t)$, $h_p(p_i | p_i^t)$, and $h_s(s | s^t)$ are quadratic functions, proving Proposition 3 is equivalent to showing their Hessians are positive definite. Also, we only focus on the positive coordinates of θ_j^t and p_i^t since other coordinates will remain zero through updates, and the proposition is vacuously true. By (S.3), (S.11), and (S.15), these Hessians are

$\mathbf{D}(\boldsymbol{\theta}_j^t)$, $\mathbf{D}(\mathbf{p}_i^t)$, and $\mathbf{D}(\mathbf{s}^t)$ respectively. Since they are all diagonal matrices, we want to show that their diagonal values are all positive.

For $\mathbf{D}(\boldsymbol{\theta}_j^t)$, we have $D(\boldsymbol{\theta}_j^t)_{kk} = \mathbf{d}(\boldsymbol{\theta}_j^t)_k = \frac{(\mathbf{A}\boldsymbol{\theta}_j^t)_k}{\theta_{jk}^t}$. The denominator of $D(\boldsymbol{\theta}_j^t)_{kk}$ is positive. Dropping the index j , its numerator is

$$\begin{aligned} \{(\text{diag}(\mathbf{s})\mathbf{P}\mathbf{P}^\top\text{diag}(\mathbf{s}) + mn(\alpha_1\mathbf{V} + \alpha_2\mathbf{V}^c))\boldsymbol{\theta}_j^t\}_k &\geq \{mn(\alpha_1\mathbf{V} + \alpha_2\mathbf{V}^c)\boldsymbol{\theta}_j^t\}_k \\ &\geq mn\min(\alpha_1, \alpha_2)\theta_{jk}^t > 0, \end{aligned}$$

since $\mathbf{V} + \mathbf{V}^c = \mathbf{I}$. Hence, $D(\boldsymbol{\theta}_j^t)_{kk}$ is positive.

For $\mathbf{D}(\mathbf{p}_i^t)$, from (S.9) and (S.10), we also have $D(\mathbf{p}_i^t)_{kk} = \mathbf{d}(\mathbf{p}_i^t)_k = \frac{(\mathbf{C}\mathbf{p}_i^t)_k}{p_{ki}^t}$. Likewise, the denominator is positive, and the numerator after dropping the index i is

$$\begin{aligned} \{(\text{diag}(\mathbf{s})\Theta^\top\Theta\text{diag}(\mathbf{s}) + mn\beta\rho^{-1})\mathbf{p}_i^t\}_k &\geq (mn\beta\rho^{-1}\mathbf{p}_i^t)_k \\ &= mn\beta r_k^{-1}p_{ki}^t > 0. \end{aligned}$$

Lastly, $D(\mathbf{s}^t)_{kk}$ is already shown to be positive from the conclusion of (S.20). This completes the proof of Proposition 3.

To finally prove Theorem 1, we combine the results of Propositions 1-3, and apply these conclusions to Theorem 2(b) in [3]. This way, we have shown that Algorithm 1 converges to a set of stationary points of $f(\Theta, \mathbf{s}, \mathbf{P})$.

D. Additional Discussion on Cross-Validation

We wish to discuss our particular design of the CV steps in Section 2.4. In particular, the calculation of $\hat{\mathbf{P}}^{(b)}$ is through NNLS instead of a re-application of ARTdeConv. This is different from the conventional design in a regression framework. We argue that this is necessary because firstly, when applied to the whole \mathbf{Y} , ARTdeConv produces a single $\hat{\Theta}$ and a single \mathbf{s} shared between all samples, and therefore a single estimate of Θ should be shared between the training set and the test set, for which we use $(\tilde{\Theta}^{(b)}, \tilde{\mathbf{s}}^{(b)})$ and NNLS to enforce this rationale. On the other hand, a re-application of ARTdeConv might produce a different Θ and/or \mathbf{s} estimate on the test set. Secondly, if the ARTdeConv model (1) represents the data well on both training and test sets and the tuning parameters are well chosen for the training set, then heuristically NNLS suffices to produce a $\hat{\mathbf{P}}^{(b)}$ close to its optimal value in terms of mean squared errors. We also note that [6] has shown through their simulations that when the deconvolution model is well held, prediction errors in \mathbf{Y} correlate highly with prediction errors in \mathbf{P} (see Figure 2 of [6]), which provides additional justifications for our design choice of the NNLS step.

E. Supplementary Information for The Simulated Pseudo-Bulk Data

E.1. Data Generation

For $k = 1, 2, \dots, 5$, s_k^* was generated independently from a χ^2 distribution with 5 degrees of freedom. For the rare class and each $i = 1, 2, \dots, n$, $\mathbf{p}_i^* \stackrel{i.i.d.}{\sim} \text{Dir}(2^5, 2^4, 2^3, 2^2, 2)$, where Dir represents the Dirichlet distribution. For the uniform class, we first drew $\boldsymbol{\alpha}_i$ from

$\alpha_{ik} \stackrel{i.i.d.}{\sim} U(0.3, 0.7)$, $k = 1, \dots, 5$, and then generated \mathbf{p}_i^* from $\text{Dir}(\boldsymbol{\alpha}_i)$. For the extra class, $\mathbf{p}_i^* \stackrel{i.i.d.}{\sim} \text{dir}(2, 2^2, 2^3, 2^4, 2^5)$, in reverse of the rare class.

For experiments where the simulated signature matrix is assumed accurate, to generate values in Θ^* , for each gene $j = 1, 2, \dots, M$, a 5×1 vector of expression was generated by

$$\boldsymbol{\theta}_j^{*\top} \sim \Pi \left[\chi_{200}^2 \cdot \{(1 - \gamma) \text{Dir}(1, 1, \dots, 1) + \gamma \text{Dir}(1, \dots, 1, 5)\} \right],$$

where $\Pi(\cdot)$ is the sampling without replacement operator. $\Pi(\cdot)$ allowed all CT1-CT5 have a number of gene signatures. On the other hand, when errors were presumed in the signature matrix when it was derived from reference gene expression and $\gamma = 1$ was assumed, the j -th row of the observed signature matrix Θ° was generated via

$$\begin{aligned} \boldsymbol{\theta}_j^{*\top} &\sim \Pi \left\{ \chi_{200}^2 \cdot \text{Dir}(1, \dots, 1, 5) \right\}, \\ \delta_{jk} &\sim \eta \cdot \text{IG}(1, 1), \quad k = 1, \dots, 5, \\ \boldsymbol{\theta}_j^{\circ\top} &= \boldsymbol{\theta}_j^{*\top} + \boldsymbol{\delta}_j. \end{aligned}$$

Here, $\boldsymbol{\delta}_j$ is a 5×1 vector with each element generated independently as above, and $\text{IG}(1, 1)$ denotes an inverse Gaussian distribution with 1 as both the mean and the shape parameters. An inverse Gaussian distribution has the property that the majority of its density is concentrated near 0. The parameter η controls the mean and variance of the signature matrix errors. The larger the η , the larger the mean and variance of the errors: the errors are basically negligible in the observed signature matrix from the truth when $\eta = 1$, while when $\eta = 200$ the errors are very strong (basically having the same mean as the true underlying expression of the gene signatures and a even higher variance), which is an extreme situation that signals huge discrepancies between the observed and the true underlying expression of selected gene signatures. The first four columns of Θ° were used as the observed partial signature matrix $\Theta_{K_0}^\circ$.

For scenarios where the reference parameters in \mathbf{m}/\mathbf{r} and therefore $\mathbf{M}/\boldsymbol{\rho}$ are presumed to be inaccurate in their relative values, we fix $\gamma = 1$ and set up the true underlying Θ^* and \mathbf{P}^* as described above. We obtain the true reference medians and ranges (m_1, \dots, m_5) and ranges (r_1, \dots, r_5) from each row of \mathbf{P}^* . We let the observed medians and ranges of CT1-CT4 proportions be shrunken from the true references by $\xi \in (0, 1)$. That is, $m_k^* = (1 - \xi)m_k$ and $r_k^* = (1 - \xi)r_k$ for $k = 1, \dots, 4$. For CT5, we set $m_5^* = \max(0, 1 - \sum_{l=1}^4 m_l^*)$. The range of CT5 after the proportions of CT1-CT4 are shrunken is not immediately clear but is definitely inflated. To this end, we think $r_5^* = r_5/(1 - \xi)$ can sufficiently represent this inflation. We can see that, the larger the magnitude of ξ , the more inaccurate the information we have on the absolute proportions of CT1-CT5. On the other hand, one might want to consider when the proportions of CT1-CT4 are inflated by ξ . However, this is completely symmetric to the case where they are shrunken in our model design (due to the L_2 norm in the penalty term) as well as in the simulation setups (as we consider three classes of CT5 absolute abundances already).

The random errors in the bulk expression $\boldsymbol{\epsilon}$ were generated based on the principle of mean-variance dependency in gene expression data: the higher the mean of a gene's expression, the higher their variation [7]. For each gene j , its error-free mean of bulk expression \bar{y}_j was calculated. Then its associated error for each sample i was generated by $e_{ji} \stackrel{i.i.d.}{\sim} N(0, \sigma^2 \bar{y}_j^2)$, $i = 1, 2, \dots, n$.

E.2. Method For Selecting Highly Cell-Type-Specific Genes

First, for each gene, the cell type for which it had the highest expression was picked as the target cell type. This gene then became a candidate for a marker of this target cell type. Second, for each candidate marker, the ratio of expression in its target cell type to those in the cell type with the second highest expression was calculated. Third, for each cell type, its candidate marker genes were ranked by the ratio calculated in the second step from highest to lowest. Finally, the top 100 candidate marker genes for each cell type were selected.

E.3. Tuning Grid And Algorithm Parameters

Cross-validation (CV) was performed in each simulation to find the best values for α_1 and β according to Section 2.4. A tuning grid $\mathfrak{A}_1 = \mathfrak{B} = (10^{-2}, 10^{-1}, \dots, 10^3, 10^4)$ was set up with the tolerance parameter chosen as $\delta = 10^{-5}$.

E.4. Matching The Estimated Proportions to Cell Types For Reference-Free Methods

We utilized $\hat{\Theta}$ and the partial signature matrix $\Theta_{K_0}^*$. Starting from the first column of $\Theta_{K_0}^*$, $\theta_{K_{01}}^*$, we found the column of $\hat{\Theta}$, say column k , that had the highest Pearson's correlation with $\theta_{K_{01}}^*$. Then, the k -th row of \hat{P} was determined to be estimated proportions for CT1. We did this for the rest of the columns of $\Theta_{K_0}^*$ and those of $\hat{\Theta}$, until there was one last unmatched column in $\hat{\Theta}$. That unmatched column, and its corresponding row in \hat{P} , were then matched to CT5.

F. Supplementary Method And Results For The Deconvolution of Bulk PBMC Samples from The Human Influenza Vaccine Study

F.1. Data Processing

FASTQ files containing 50bp (base pairs) pair-end raw nucleotide sequence reads of transcripts from Illumina Hiseq 2000 sequencers were downloaded from the Sequence Read Archive (SRA) BioProject PRJNA271578. The raw reads were pre-processed and filtered where reads with length < 50bp, with > 30% bases with quality scores < 30, having an average quality score < 25 in any 10bp interval, or corresponding to special adapter sequences were removed using the software `fastp` [8]. Then, reads passing the filters were mapped to reference human genome hg38 GRCh38 Release 43 (downloaded from the GENCODE website) and quantified using `salmon` [9]. The output files were then processed using the R package `tximport` [10]: only protein-coding genes with an official gene symbol were selected and their transcripts per million (TPM) values were gathered into a gene-by-sample matrix of gene expression. Additionally, genes with a total TPM of less than 10 across the four cell types were excluded from consideration.

Distinct marker genes for the four cell types were individually selected for each subject using sorted bulk profiles of individual cell types. The selection process identified the top

10 genes exhibiting the highest cell-type specificity for each cell type from each subject according the ratio of expression method outlined in Section 3.1. The union of the two sets of marker genes, totalling 73 genes, were used in the deconvolution.

F.2. Calculating Reference PBMC Proportion Medians and Ranges from External Data

To calculate the reference PBMC cell-type proportion medians and ranges in Table 1, we adopted the data from [11], a highly cited textbook on PBMC. The median and range for the cell types with reference expression were calculated through the descriptions in the textbook using a simple method. For example, the book states that lymphocytes account for 70% - 90% of all PBMCs, and among the lymphocytes 70% - 85% are T cells. Thus, the range of T cell percentage among PBMCs is 49% - 76.5%, or 0.49 - 0.765 in proportion. The median is thus $(0.49 + 0.765)/2 = 0.6275$ and the range is $0.765 - 0.49 = 0.275$, corresponding to the reference values for T cell in Table 1. The reference values for B cell, NK cell, and monocyte were similarly calculated. For the “other cells”, their median proportion is $1 - (0.6275 + 0.0625 + 0.1075 + 0.15) = 0.0525$. As for the ranges, the upper limit of the proportion for “other cells” occurs under the lower limit of lymphocytes and monocyte, which according to [11] is $1 - (0.7 + 0.1) = 0.2$ (70% lymphocyte, which includes T cell, B cell, and NK cell combined, and 10% monocyte), while the lower limit is 0 (when there are 90% lymphocyte and 20% monocyte, an impossible scenario). This leads to a range of 0.2.

We notice a range of 0.2 could be a little wide for “other cells”. As it turned out, these coarse parameters for medians and ranges sufficed for ARTdeConv to work properly. Thus, it is not always necessary to obtain super accurate reference parameters as long as they are in the right orders of magnitude.

F.3. Tuning Grid And Algorithm Parameters

A random seed of 1000 was set in the R programming environment. The tuning grid for α_1 was set as the interval from 2^{-5} to 2^0 with a step size of 0.2 in the power, and that for β was set as the interval from 2^0 to 2^5 also with a step size of 0.2 in the power. α_2 was fixed at 10^{-12} . The difference in magnitudes between α_1 and β in the tuning grids ensured proper regularization, for there was a scale difference between gene expression and the proportions. A 4-fold cross-validation was invoked to choose the optimal tuning parameters. The eventual selected tuning parameter values were within the boundaries of the grids. The tolerance parameter was set as $\delta = 10^{-4}$.

F.4. Fixing mRNA Amounts as One For All Cell Types using ARTdeConv Results in Biased Deconvolution Results

In Section 3.2, it was posited that bulk and gene signature matrices whose expression values were measured in TPM would lose the information on cell-type mRNA amounts, necessitating the inclusion of s described in the underlying model (1). To verify this claim, we re-ran the data analysis on the same data in TPM as in Section 3.2 using the same empirical estimates M and ρ , the same tolerance parameter, and the same tuning grid for the hyperparameters, and the same random seed, but coerced $\text{diag}(s)$ to be the identity matrix (i.e. coerced the cell-type mRNA amounts to 1) throughout updates in

Algorithm 1. We observed that the estimated proportions for PBMC cell types for both samples on Day 0 deviates more from those measured by flow cytometry when compared to when $\text{diag}(\mathbf{s})$ is not coerced, as shown in Figure 4b.

Supplementary Table 1: Means and ranges of PBMC cell type proportions calculated from the reference values.

	T cells	B cells	NK cells	Monocytes	Other cells
Means	0.6275	0.0625	0.1075	0.15	0.0525
Ranges	0.275	0.055	0.145	0.1	0.2

G. Supplementary Method And Results For The Deconvolution of Bulk PBMC Samples from The COVID-19 Study

G.1. Study Design And Data Processing

The dataset generated from the study of [12] and downloaded using NCBI GEO accession number GSE152418 contained 34 subjects recruited from Atlanta, GA, USA. It included gene expression from human blood PBMC bulks samples collected from 17 healthy control subjects, one convalescent subject, and 16 subjects diagnosed with COVID-19. Healthy controls were asymptomatic adults whose samples were collected before the widespread circulation of SARS-CoV-2 virus in the community. Subjects with COVID-19 diagnosis were further classified into three levels of disease severity based on the based on the adaptation of the Sixth Revised Trial Version of the Novel Coronavirus Pneumonia Diagnosis and Treatment Guidance. Moderate cases were defined as respiratory symptoms with radiological findings of pneumonia. Severe cases were defined as requiring supplemental oxygen, and ICU-hospitalized cases were those in critical conditions who needed ICU care due to organ failures.

The gene symbols were annotated to 24,259 genes using the gconvert method of the **gProfileR** package in R software. The raw counts were then converted to counts per million (CPM) using those annotated genes. Among the 16 samples from COVID-19 subjects, two (labeled S155 and S179) contained abnormally high levels of *HBB* expression (namely, *HBB* was the most highly expressed gene in those two samples; results are not shown), which could only been found in red blood cells and suggested sample contamination. Therefore, these two samples were removed from the deconvolution procedures. This also led to S155, which also provided the study with single cell samples, being excluded from the comparison in Figure 5d. The one convalescent sample was also excluded due to its unique designation.

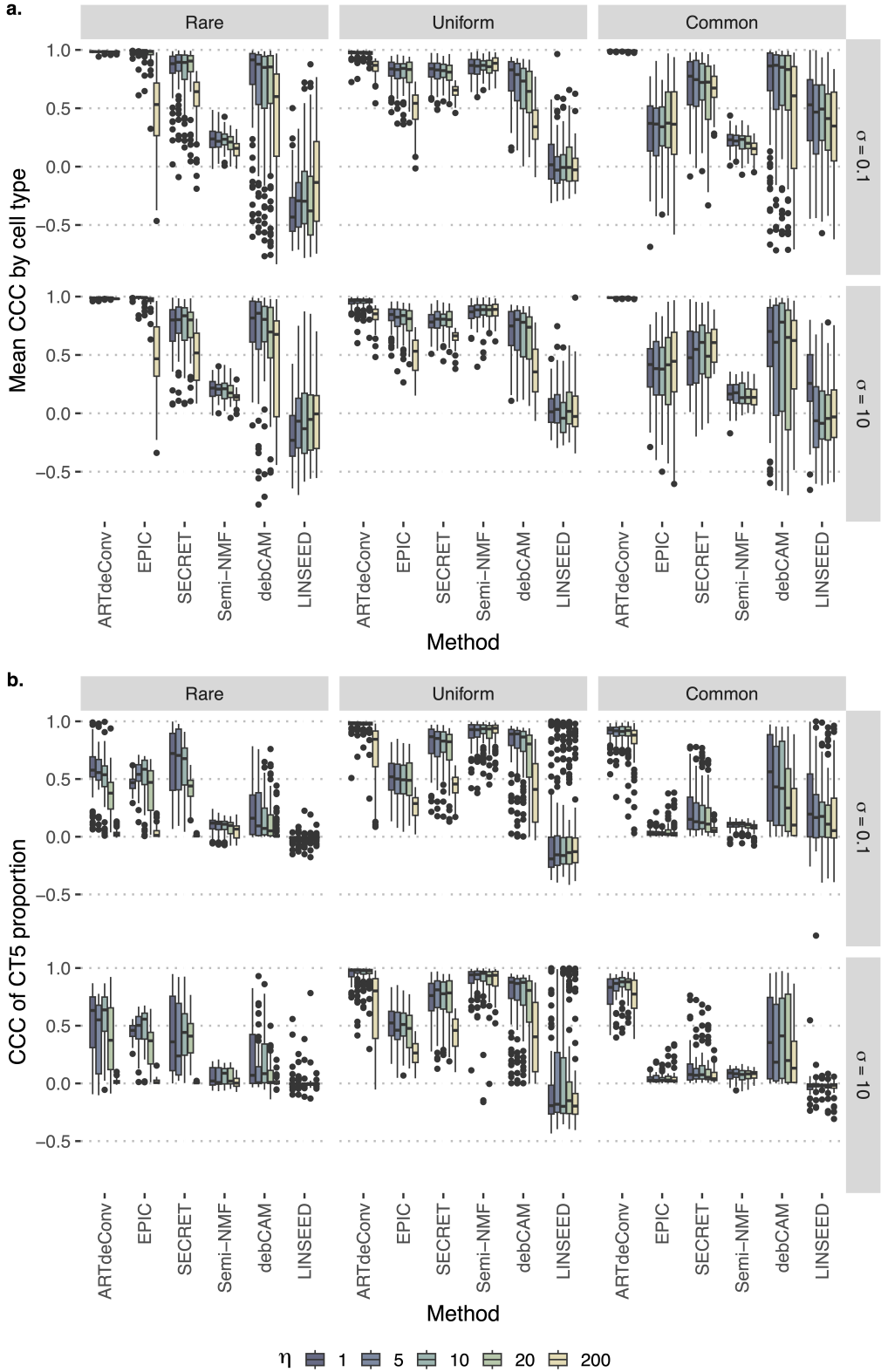
The scRNA-seq data were generated by [12] using CITE-seq of >63,000 cell samples from five healthy controls and seven COVID-19 diagnosed patients. Of the seven patients, three were labeled as moderate cases, three severe cases, and one requiring ICU care. Notably, dendritic cells were enriched by the experimenters and mixed back into the samples for CITE-seq. All five healthy subjects and six of the seven (except S155, which were previously excluded) had measured bulk gene expression from independent PBMC samples as well for the analysis. To process the raw scRNA-seq data downloaded from

GEO accession GSE155673, we first merged the single cell gene expression from all 12 subjects together in R package `Seurat` V4 [13]. We then performed a quality control procedure for the cells, retaining those with a detected number of genes per cell between 200 and 5000 and filtering out cells with >15% mitochondrial counts. Genes with total expression less or equal to 2 across all cell samples were removed as well. We applied the global-scaling normalization method `LogNormalize` to normalize the feature expression measurements for each cell by the total expression, multiplied this by a scale factor of 10^6 , and log-transformed the result. We employed the UMAP dimensional reduction technique to determine the cell type notation. The R package `SingleR` [14] was used for the final determination of cell types, using gene signature data from [15] as the cell type reference. The single-cell data input now has genes as rows and estimated cell type notations with subjects as columns. In the end, 41,146 cells and 26,531 genes were retained in the gene-by-cell expression matrix of all 12 samples.

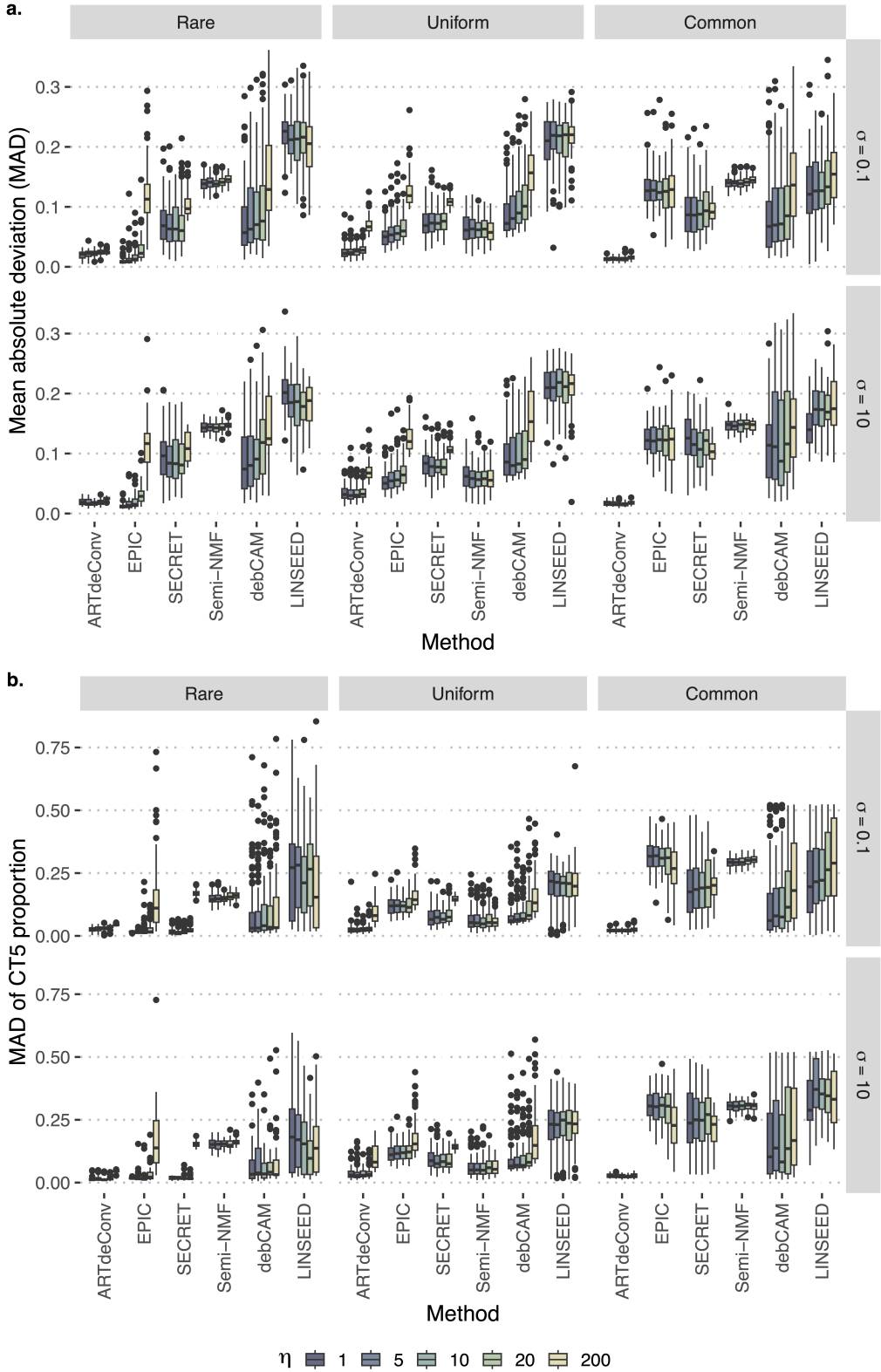
We then separated the gene-by-cell matrix into two matrices, one containing only cells from healthy controls (23,531 cells) and the other only those from COVID-19 subjects (17,615 cells). Due to the limits of memory allocations to CIBERSORTx users, 11,765 cells from healthy controls were randomly sampled for each cell type proportionally to its original relative abundance. The cell types were re-grouped by merging all cell subsets of the four major cell types of interest together. The cellular gene expression from cells not belonging to any of the four cell types were discarded for gene signature generation. The processed sub-matrices were then separately sent to CIBERSORTx software’s Create Signature Matrix module [16] to obtain gene signature matrices for both control and COVID-19 cell samples. The signature matrix for healthy controls contains 1,368 genes for the four cell types, while that for COVID-19 samples contains 1,388 genes. After matching the common genes from the bulk expression matrices and the signature matrices returned from CIBERSORTx, there were 1,280 genes for the deconvolution of healthy control samples and 1,297 genes for the deconvolution of COVID-19 patient samples.

G.2. Tuning Grid And Algorithm Parameters

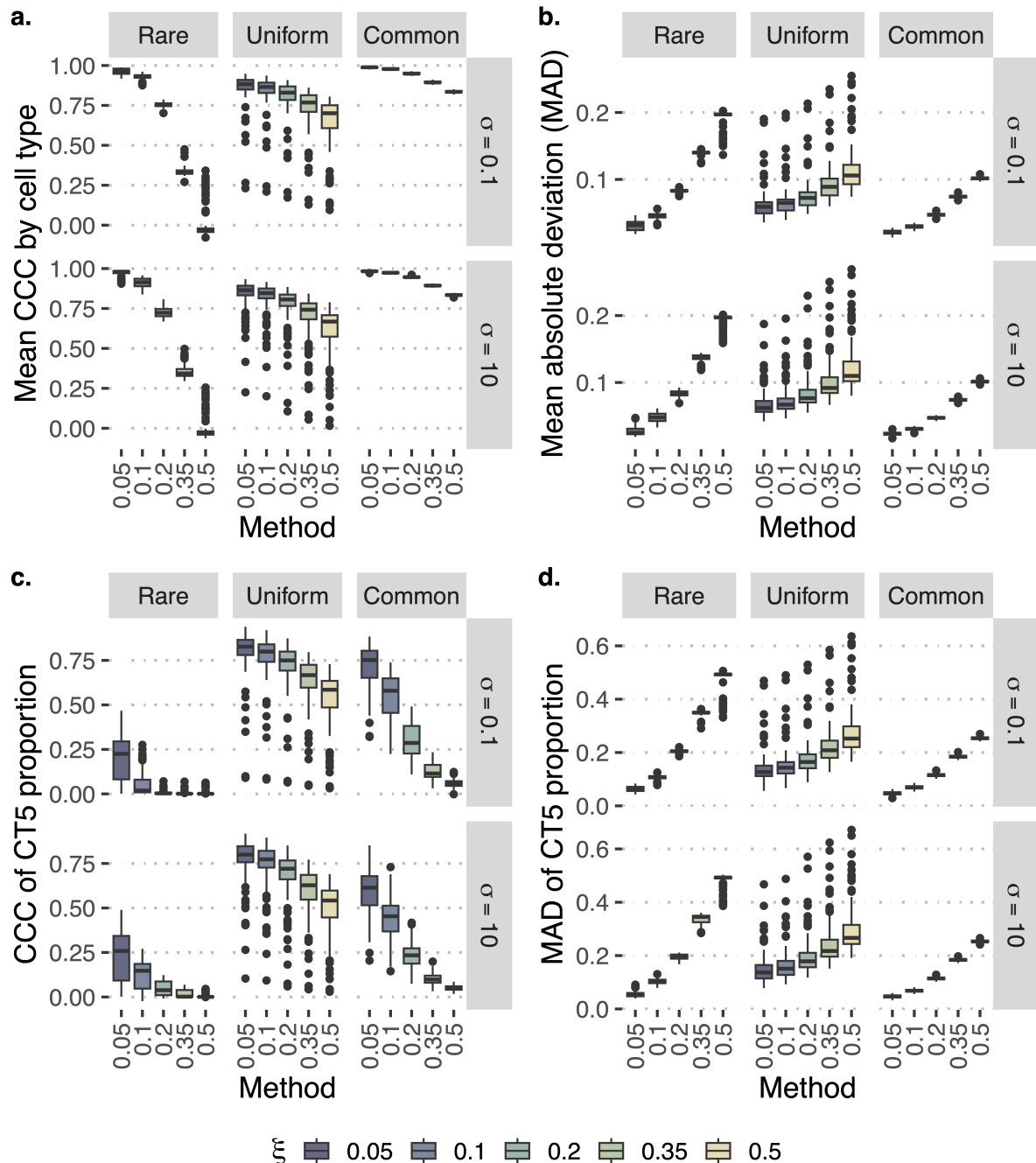
We adopted a tuning grid and a set of parameters for ARTdeConv to the settings in Supplementary Material Section F.3 for the analysis in Section 3.2. A random seed of 1000 was set in the R programming environment. For the deconvolution of healthy control samples, the tuning grid for α_1 was set as the interval from 2^{-3} to 2^1 with a step size of 0.2 in the power, and that for β was set as the interval from 2^2 to 2^6 also with a step size of 0.2 in the power. α_2 was fixed at 10^{-12} . For that of COVID-19 infected samples, the tuning grid for α_1 was set as the interval from 2^{-4} to 2^0 with a step size of 0.2 in the power, and that for β was also set as the interval from 2^2 to 2^6 also with a step size of 0.2 in the power. α_2 was again fixed at 10^{-12} . A 4-fold cross-validation was invoked in both deconvolution analyses to choose the optimal tuning parameters. The eventual selected tuning parameter values were within the boundaries of the grids in each case. The tolerance parameter was set as $\delta = 10^{-4}$.



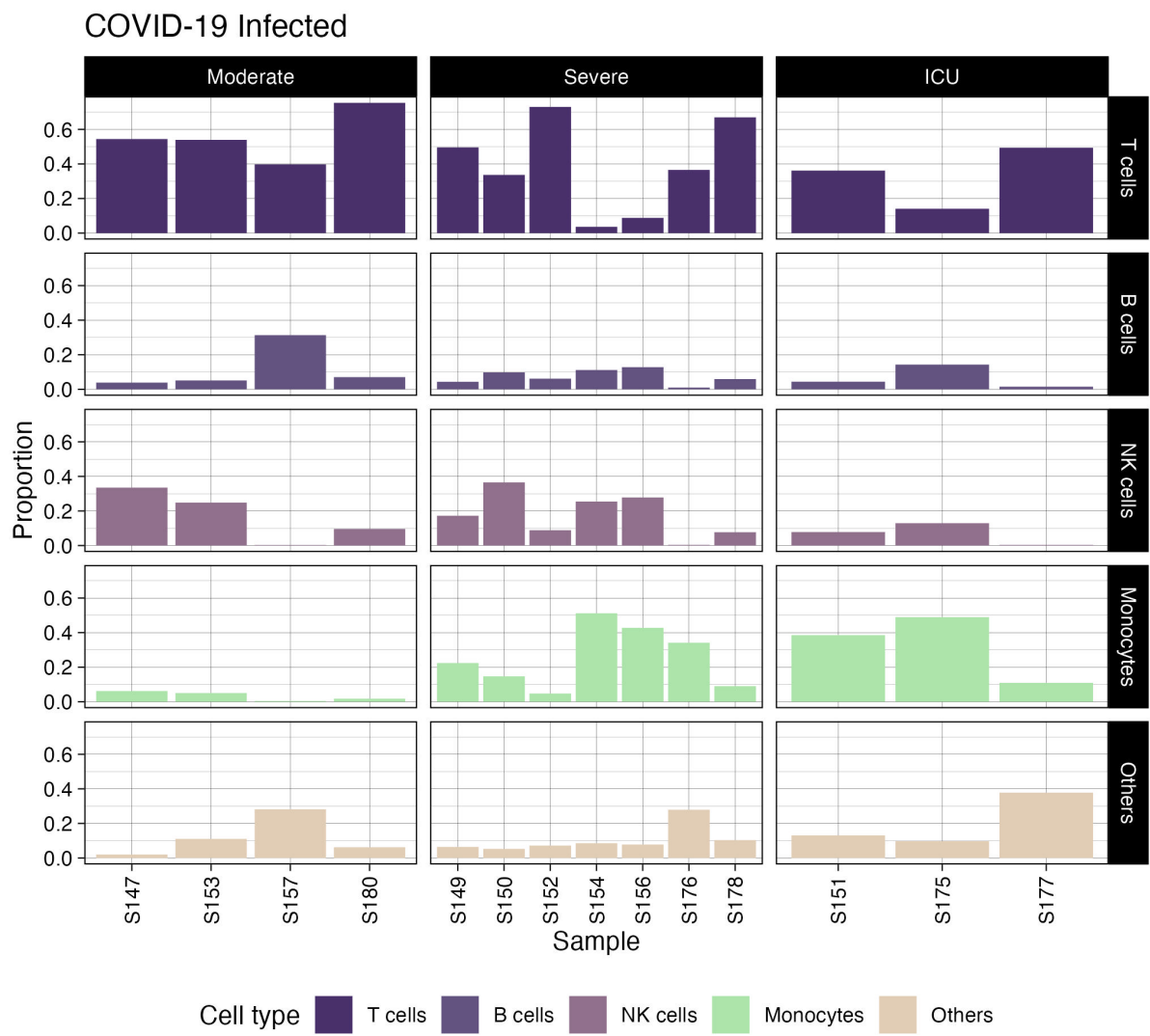
Supplementary Figure 1: **a.** Mean Concordance Correlation Coefficient (CCC) by cell type between true proportions and estimated cell-type proportions from pseudo-bulks for the simulations where the observed signature matrix is differed from the truth. **b.** CCC between estimated and true proportions of CT5 in the pseudo-bulks. Each column represents a case of the relative abundance of CT5 against other cell types in the simulated pseudo-bulks. Each row represents the level of random noises controlled by σ . Colors represent different levels of deviation from the truths in Θ^* regulated by η . The larger the η , the more the deviation.



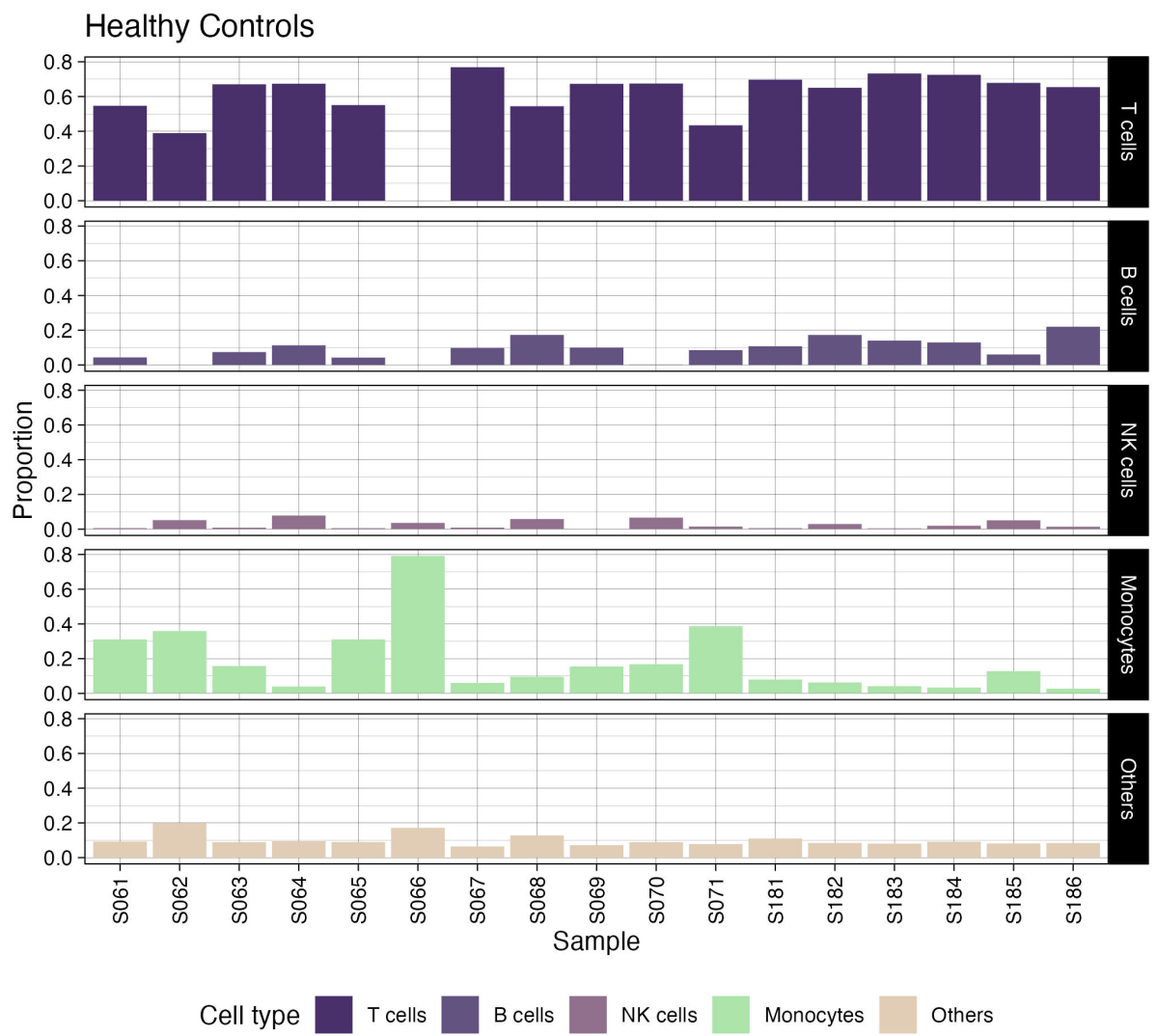
Supplementary Figure 2: **a.** Mean Absolute Deviation (MAD) by cell type between true proportions and estimated cell-type proportions from pseudo-bulks for the simulations where the observed signature matrix is differed from the truth. **b.** MAD between estimated and true proportions of CT5 in the pseudo-bulks. Each column represents a case of the relative abundance of CT5 against other cell types in the simulated pseudo-bulks. Each row represents the level of random noises controlled by σ . Colors represent different levels of deviation from the truths in Θ^* regulated by η . The larger the η , the more the deviation.



Supplementary Figure 3: **a.** Mean Concordance Correlation Coefficient (CCC) by cell type between true proportions and estimated cell-type proportions from pseudo-bulks for the simulations where the observed reference median and range parameters are differed from the truths. **b.** Mean Absolute Deviation (MAD) by cell type between true proportions and estimated cell-type proportions from pseudo-bulks. **c.** CCC between estimated and true proportions of CT5 in the pseudo-bulks. **d.** MAD between estimated and true proportions of CT5 in the pseudo-bulks. Each column represents a case of the relative abundance of CT5 against other cell types in the simulated pseudo-bulks. Each row represents the level of random noises controlled by σ . Colors represent different levels of deviation from the truths in reference parameters regulated by ξ . The larger the ξ , the more the deviation.

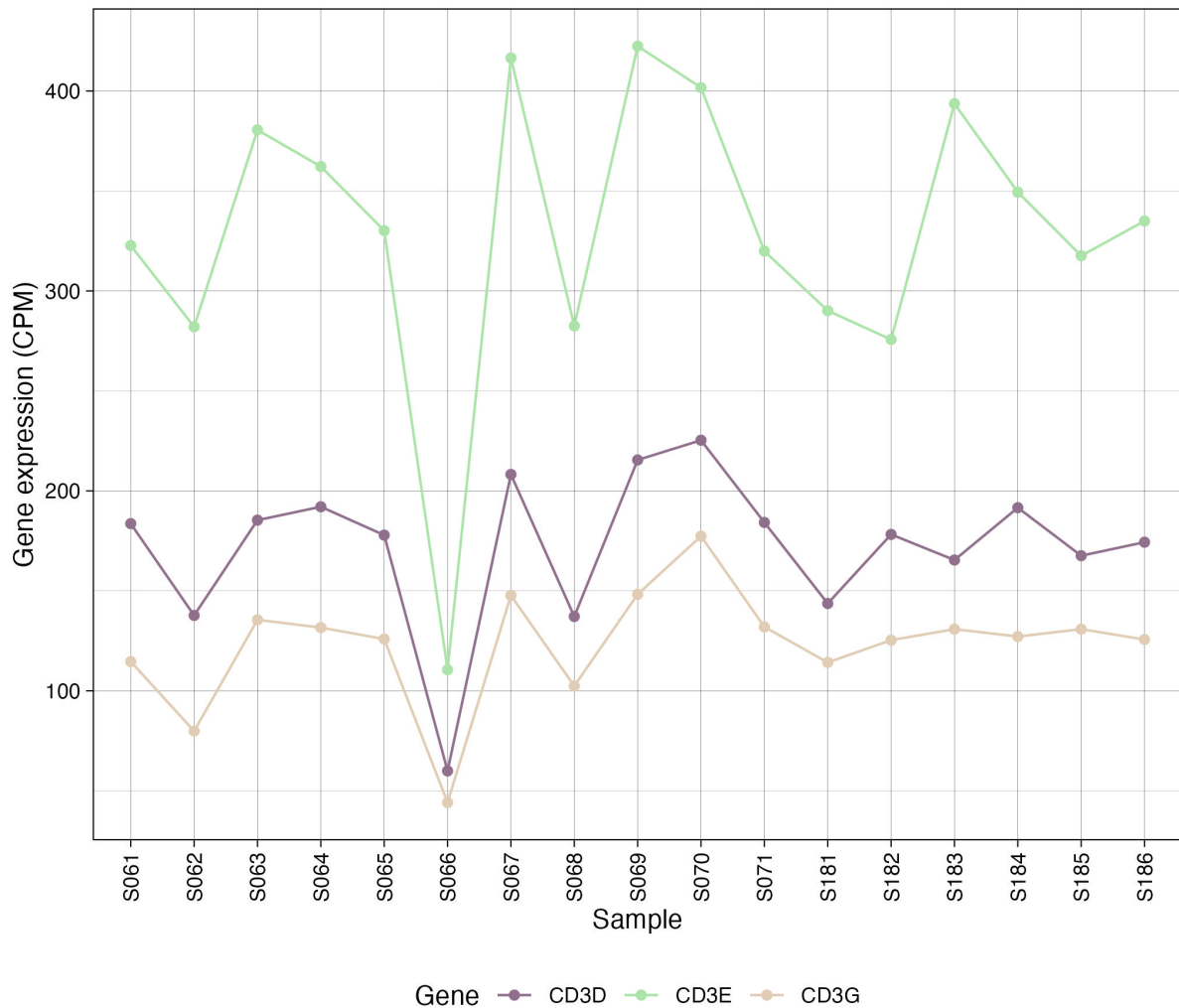


Supplementary Figure 4: Bar graphs of the deconvolved cell type proportions of all COVID-19 infected samples, grouped by their classified disease severity



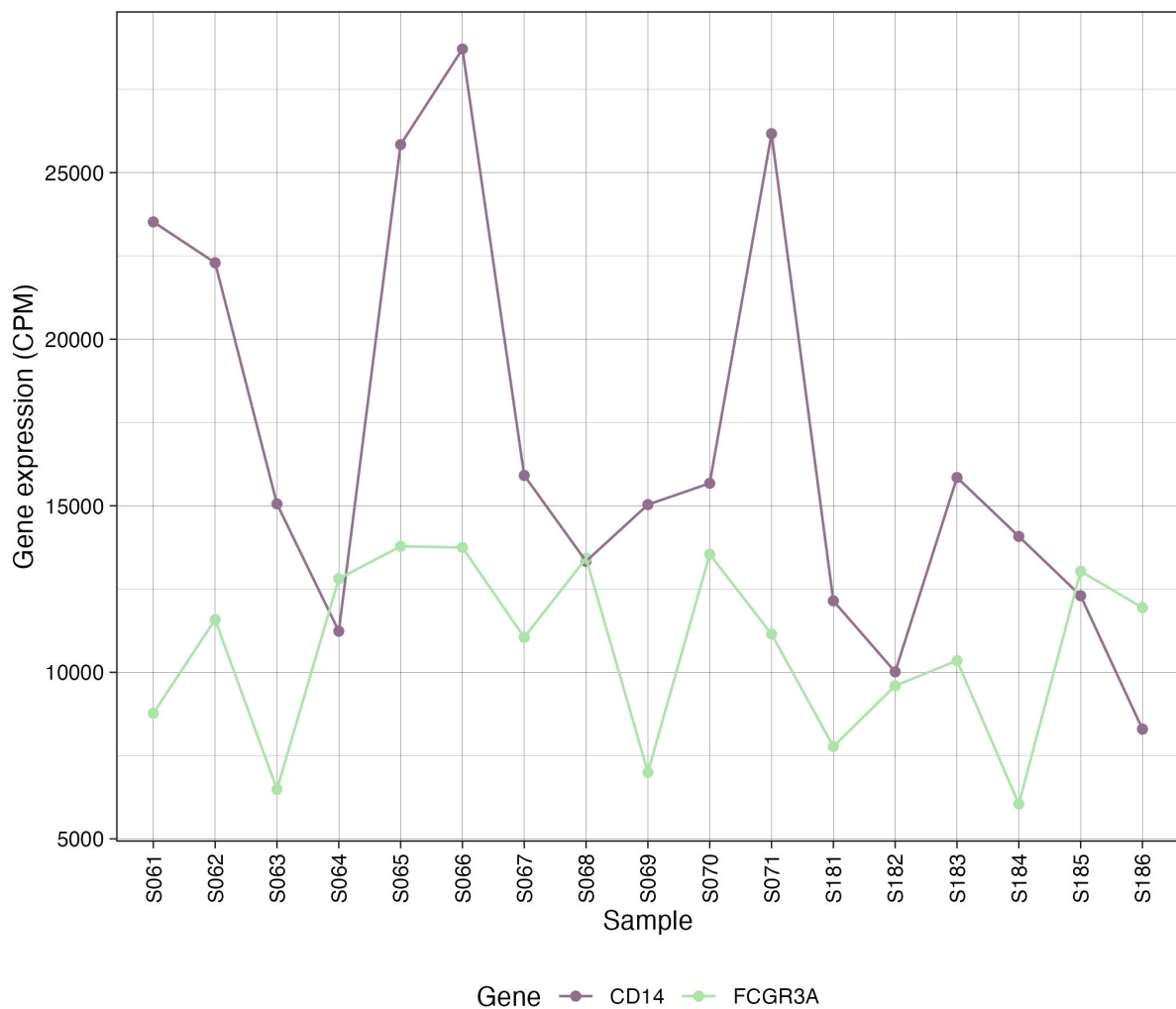
Supplementary Figure 5: Bar graphs of the deconvolved cell type proportions of all healthy control samples.

Low Expression of CD3 Genes in S066



Supplementary Figure 6: Expression of *CD3* genes, the translation of which produces T cells' CD3 markers, among healthy samples with exceptionally low expression observed in sample S066.

High Expression of CD14 Genes in S066



Supplementary Figure 7: Expression of *CD14* and *FCGR3A* genes among healthy samples with high *CD14* expression observed in sample S066. *CD14* is responsible for the production of CD14 surface markers on classical/intermediate monocytes and *FCGR3A* responsible for that of CD16 surface markers on non-classical/intermediate monocytes.

References

- [1] Lee, D., & Seung, H. S. (2000). *Algorithms for non-negative matrix factorization*. In *Advances in neural information processing systems*, 13.
- [2] Lin, C.-J. (2007). *On the convergence of multiplicative update algorithms for nonnegative matrix factorization*. *IEEE Transactions on Neural Networks*, 18(6), 1589–1596.
- [3] Razaviyayn, M., Hong, M., & Luo, Z.-Q. (2013). *A unified convergence analysis of block successive minimization methods for nonsmooth optimization*. *SIAM Journal on Optimization*, 23(2), 1126–1153.
- [4] Kim, J., He, Y., & Park, H. (2014). *Algorithms for nonnegative matrix and tensor factorizations: A unified view based on block coordinate descent framework*. *Journal of Global Optimization*, 58(2), 285–319.
- [5] Lange, K. (2016). *MM optimization algorithms*.
- [6] Dong, M., Thennavan, A., Urrutia, E., Li, Y., Perou, C. M., Zou, F., and Jiang, Y.. *SCDC: bulk gene expression deconvolution by multiple single-cell RNA sequencing references*. *Briefings in Bioinformatics*, 22(1):416–427, Jan. 2021.
- [7] Anders, S. & Huber, W (2010). *Differential expression analysis for sequence count data*. *Nature Precedings*, pages 1–1.
- [8] Chen, S., Zhou, Y., Chen, Y., & Gu, J. (2018). *fastp: an ultra-fast all-in-one fastq preprocessor*. *Bioinformatics*, 34(17):i884–i890.
- [9] Patro, R., Duggal, G., Love, M. I., Irizarry, R. A., & Kingsford C. (2017). *Salmon provides fast and bias-aware quantification of transcript expression*. *Nature methods*, 14(4):417–419.
- [10] Soneson C., Love M. I., & Robinson M. D. (2015). *Differential analyses for rna-seq: transcript-level estimates improve gene-level inferences*. *F1000Research*, 4.
- [11] Kleiveland, C. R. (2015). *Peripheral Blood Mononuclear Cells*. In K. Verhoeckx et al. (Ed.), *The Impact of Food Bioactives on Health: in vitro and ex vivo models [Internet]*. Springer.
- [12] Arunachalam, P. S., Wimmers F., Mok C. K. P., Perera R. A. P. M., Scott M., Hagan T., Sigal N., et al. (2020). *Systems Biological Assessment of Immunity to Mild versus Severe COVID-19 Infection in Humans*. *Science* 369 (6508): 1210–20.
- [13] Hao, Y., Hao, S., Andersen-Nissen, E., Mauck, W. M., 3rd, Zheng, S., Butler, A., Lee, M. J., Wilk, A. J., Darby, C., Zager, M., Hoffman, P., Stoeckius, M., Papalexi, E., Mimitou, E. P., Jain, J., Srivastava, A., Stuart, T., Fleming, L. M., Yeung, B., ... Satija, R. (2021). *Integrated analysis of multimodal single-cell data*. *Cell*, 184(13), 3573–3587.e29.
- [14] Aran, D., Looney, A. P., Liu, L., Wu, E., Fong, V., Hsu, A., Chak, S., Naikawadi, R. P., Wolters, P. J., Abate, A. R., Butte, A. J., & Bhattacharya, M. (2019). *Reference-based analysis of lung single-cell sequencing reveals a transitional profibrotic macrophage*. *Nature Immunology*, 20(2), 163–172.

- [15] Monaco, G., Lee, B., Xu, W., Mustafah, S., Hwang, Y. Y., Carré, C., Burdin, N., Visan, L., Ceccarelli, M., Poidinger, M., Zippelius, A., Pedro de Magalhaes, J., & Larbi, A. (2019). *RNA-Seq Signatures Normalized by mRNA Abundance Allow Absolute Deconvolution of Human Immune Cell Types*. *Cell Reports*, 26(6), 1627–1640.e7.
- [16] Newman, A. M., Steen, C. B., Liu, C. L., Gentles, A. J., Chaudhuri, A. A., Scherer, F., Khodadoust, M. S., Esfahani, M. S., Luca, B. A., Steiner, D., Diehn, M., & Alizadeh, A. A. (2019). *Determining cell type abundance and expression from bulk tissues with digital cytometry*. *Nature Biotechnology*, 37(7), 773–782.